Post-processing Techniques for Polarimetric Passive Millimeter Wave Imagery

L. Wu [1,2], J. Q. Zhu [1], S. S. Peng [1], Z. L. Xiao [1], and Y. K. Wang [1]

[1] School of Electronic and Optical Engineering
Nanjing University of Science & Technology, Nanjing, 210094, China
li_wu@njust.edu.cn, zhujiaqi3301@163.com, pengshusheng@njust.edu.cn, zelongxiao@njust.edu.cn, wykkerry@163.com

[2] Ministerial Key Laboratory of JGMT
Nanjing University of Science & Technology, Nanjing, 210094, China

Abstract ─ Post-processing techniques for polarimetric passive millimeter wave (MMW) imagery are proposed to display imaging information comprehensively. Initially an image fusion method based on two-scale decomposition is proposed to realize polarimetric passive imagery fusion. The fusion rules are separately designed for base layer and detail layer to reconstruct weight maps. Then an improved technique for displaying polarization information through color is proposed to present polarization features simultaneously with unpolarized imagery. Experimental results demonstrate that the proposed post-processing techniques are capable of presenting more informative imagery.

Index Terms ─ Millimeter wave passive imaging, polarimetric imaging, remote sensing.

I. INTRODUCTION

Millimeter wave (MMW) passive imaging sensor constructs the MMW images of the observed scene by recording radiometric temperature distributions. Recently passive MMW imaging sensors have been increasingly applied in a variety of fields, including security screening, surveillance and person recognition due to their ability to image through textiles, smoke, fog, light rain, dust storms [1-2]. Moreover, several polarimetric passive MMW imaging sensors have already been developed to provide polarimetric information of the observed scene [3-5].

Due to the wide applications of polarimetric passive MMW imaging system, how to process polarimetric information of objects is becoming an important research topic. Polarimetric brightness temperatures have been successfully used for remote sensing of wind speed and direction over sea surfaces [5-6]. Polarization-based techniques are presented to classify materials and acquire object surface orientation information using polarimetric passive MMW imagery [7-8]. A linear polarization sum imaging method which is based on the combination of the different polarization images is presented in [9] to increase the intensity contrast between the target area and background area. In our previous work [10], linear polarization characteristics of various terrains at MMW band for image interpretation were experimentally investigated. And it was proved that polarization has a decisive advantage over the single intensity for terrain identification.

However, there are few literatures have discussed the post-processing techniques for polarimetric passive MMW imagery collected by polarimetric imaging sensors. Siegenthaler et al. illustrated the image registration and fusion for the MMW images of 91 GHz Scanning Polarimetric Imaging Radiometer (SPIRA) and optical images [11]. A technique defined as polarization display through Color (PDC) is proposed in [12] to display polarization information from passive MMW sensors within a single image.

As the fused information is useful for the understanding enhancement of surroundings and is beneficial to human and machine vision for planning and decision-making, a method based on computationally efficient two-scale decomposition is proposed for polarimetric passive MMW imagery fusion. In addition, an improved technique for displaying polarization information through color which is capable of providing more details compared with the conventional PDC is also presented in this paper.

II. STOKES VECTOR DEFINITION

The signal received by MMW radiometer comes from the emitted radiation of objects and refracted or reflected radiation of objects and background. Therein, MMW radiation emitted by objects are not polarized. However, it differs in the reflection and refraction of

Submitted On: September 28, 2017
Accepted On: April 10, 2018

polarized radiation from various media and leads to partial polarization of radiation energy collected by MMW radiometer. Stokes parameters are commonly employed to characterize the polarization of electromagnetic wave and are well applied to describe the polarimetric information of passive MMW imagery. The expression of Stokes parameters is comprised of four elements, which can be written as:

$$\begin{pmatrix} S_0 \\ S_1 \\ S_2 \\ S_3 \end{pmatrix} = \begin{pmatrix} (T_h + T_v)/2 \\ T_v - T_h \\ T_{45^\circ} - T_{-45^\circ} \\ T_{RHC} - T_{LHC} \end{pmatrix}, \quad (1)$$

where, S_0, S_1, S_2 and S_3 represent the total intensity of radiation in all polarizations, the difference in intensity between two orthogonal linear polarization states, the degree of linear polarization at an angle of 45° to the horizontal and the degree of right-hand circular polarization respectively [5]. *T* denotes the radiometric temperature with different polarization modes, the subscripts of *h, v,* 45°, -45°, *RHC* and *LHC* represent horizontal, vertical, linear 45°, linear -45°, right-hand circular and left-hand circular polarization mode respectively.

Polarimetric passive MMW imaging systems are usually constructed with incoherent or coherent methods. For the incoherent PMMW imaging system, it requires simpler hardware with one receiver, thus it cannot measure Stokes parameters simultaneously. One the other hand, correlation polarimetric MMW system with parallel receivers is preferable to measure all Stokes parameters at a time. But the additional components will lead to higher cost and decreased performance of imaging system. To make that the proposed techniques can be applied to both incoherent and coherent imaging systems, the first two Stokes parameters, i.e., the sum and difference between the vertical and horizontal polarization states, are easily obtained for both kinds of imaging systems and thus will be processed to demonstrate the proposed post-processing techniques.

III. POST-PROCESSING TECHNIQUES

A. Polarimetric imagery fusion

It is known from the Rayleigh-Jeans law that the radiation emitted from the object is linear with the temperature at MMW frequencies, the retrieved parameter of imaging radiometer is radiometric temperature instead of intensity by calibrating the sensor with hot and cold calibration sources. So the measured Stokes parameter S_0 is the average of horizontal and vertical radiometric temperatures and it can be regarded as the unpolarized image, whereas Stokes parameter S_1 is radiometric temperature difference between the two orthogonal linear polarization states In this section, an image fusion algorithm which retains both radiometric intensity and polarimetric difference features is proposed to improve image readability. The processes sketch of the presented method for polarimetric passive MMW imagery fusion is presented in Fig. 1.

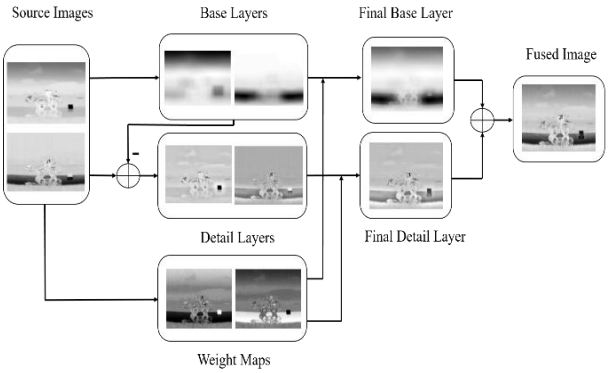

Fig. 1. Schematic diagram of the proposed fusion method for polarimetric passive MMW imagery.

An average filter based two-scale decomposition [13] is employed to decompose the polarimetric passive MMW images into the base layers and detail layers. The base layer of each source image is expressed as:

$$B_n = S_n * Z, \quad (2)$$

where S_n is the polarimetric passive MMW source image, *Z* is the average filter. The detail layer of the decomposed image can be obtained based on base layer with the following expression:

$$D_n = S_n - B_n. \quad (3)$$

By performing the above decomposition steps, each separate passive MMW image is decomposed into a base layer containing the large-scale variations in intensity and a detail layer containing the small-scale details. Based on achievements of the base layer and detail layer which correspond to the low-frequency and high-frequency components separately, the fusion of the base layer and detail layer can be respectively completed by constructing proper weights with:

$$\overline{B} = w_{S_0}^B B_{S_0} + w_{S_1}^B B_{S_1}, \quad (4)$$

$$\overline{D} = w_{S_0}^D D_{S_0} + w_{S_1}^D D_{S_1}, \quad (5)$$

where, $w_{S_0}^B$ and $w_{S_1}^B$ are the weight factors constructed for the base layer fusion, and $w_{S_0}^D$ and $w_{S_1}^D$ are the weight factors constructed for the detail layer fusion. The final fused image can be constructed by the addition of the updated base layer and the updated detail layer:

$$F = \overline{B} + \overline{D}. \quad (6)$$

The human perception system is sensitive to the contrast of visual signals, such as color, intensity and texture, and this phenomenon is regarded as the spatial attention [16]. As the low-frequency component is the

approximation of an image, the visual spatial attention based fusion rule is employed for the low-frequency component to keep the salient profiles of the both source images as much as possible. Based on the saliency map proposed in [14] which is built upon the color contrast between image pixels, a similar saliency value of a pixel P_k in image P is computed as:

$$SalS(P_k) = \sum_{\forall P_i \in P} \|P_k - P_i\|. \quad (7)$$

where, $\|\cdot\|$ denotes the radiometric temperature distance metric. Assumed that the gray value of the pixel P_k is a_m after mapping the measured radiometer temperatures linearly to range of [0,255], the above expression can be rewritten as:

$$SalS(a_m) = \sum_{n=0}^{255} f_n \|a_m - a_n\|. \quad (8)$$

where f_n denotes the frequency of pixel value a_n in the image and it can be obtained in histograms. Subsequently, the saliency maps $SalS(x,y)$ of the source images can be constructed and the fusion weight factors are determined using the following expression:

$$w_{S_0}^B(x,y) = \frac{SalS_{S_0}(x,y)}{SalS_{S_0}(x,y) + SalS_{S_1}(x,y)}, \quad (9)$$

$$w_{S_1}^B(x,y) = \frac{SalS_{S_1}(x,y)}{SalS_{S_0}(x,y) + SalS_{S_1}(x,y)}. \quad (10)$$

The detail layer of the image presents detailed features, such as texture, edge. The local energy based weighted average method is used to keep detailed information. The local energy within region *R* of each pixel in source image is given as:

$$E(x,y) = \sum_{m,n \in R} a^2(x+m, y+n), \quad (11)$$

where, $a(x,y)$ represents the gray level of the pixels. Based on the constructed local energy maps of source images, the fusion weight factors can be determined by:

$$w_{S_0}^D(x,y) = \frac{E_{S_0}(x,y)}{E_{S_0}(x,y) + E_{S_1}(x,y)}, \quad (12)$$

$$w_{S_1}^D(x,y) = \frac{E_{S_1}(x,y)}{E_{S_0}(x,y) + E_{S_1}(x,y)}. \quad (13)$$

As above, the base layer and detail layer weigh maps construction method is able to keep salient and interested features of the source images, it will lead to a better fusion performance compared to most weight factors construction methods like simply averaging of the source images.

B. Polarization information display

Though the fused image preserves the details of separate polarimetric passive MMW images, it provides less information than a color image due to the limitations of image grayscale. There is an alternative approach to display polarimetric information of passive MMW imagery with a color image determined by polarization. An example of that is the technique named PDC (polarization display through color) introduced in [12]. For the convenience of comparison, the hue, saturation, lightness cylindrical-coordinate color mapping system is used to deliver a color image in this paper as done in [12].

As the difference between the two orthogonal linear polarization states is applied to target identification in some biological systems, the imaged scene is classified into three categories by setting thresholds for the Stokes parameter S_1. Here the mean value of S_1 is employed as the offset T_{offset} which is resulted by the kinetic temperature of object. And the threshold δ is determined with the following expression:

$$\delta = (T_{med} + T_{df})/2, \quad (14)$$

where T_{med} is the median of S_1, T_{df} is the difference between T_{med} and the maximum or minimum value of S_1 which leads to a smaller number. So the pixels of image will be classified into three groups by determining the values position relative with thresholds of $T_{offset} \pm \delta$, including pixels smaller than T_{offset}-δ, pixels between T_{offset}-δ and T_{offset}+δ, and pixels larger than T_{offset}+δ. And the hue value of each pixel in the color image is assigned to one of the three different constants which would determine the color of the image depending on the classification results. As for the saturation, it is shaped with the values of Stokes parameter S_1 which are linearly scaled to a range of $[\lambda_{sat}, 1]$ for each classification. Compared with a constant saturation value, more details can be provided by the varying color saturation. At last the unpolarized image is mapped to the lightness of color mapping system, where the maximum is scaled to 1 and the minimum is scaled to 0.

IV. EXPERIMENTAL RESULTS

A. Fusion results and evaluation analysis

Several polarimetric passive MMW images collected by the raster-scanned polarimetric imaging sensor [15] are processed with the proposed method. The window size of the average filter Z in Equation (2) is set to 31*31 for numerical results as suggested in [13], [18]. And the size of region *R* in Equation (11) is 2*2 to obtain optimal comprehensive performances. A scene of the experiment is shown in Fig. 2 (d). It can be seen that a digger is adjacent to an asphalt road which went laterally across the lawn. A metal plate with a tilting angle of 45° to the horizon is put on the right side of the vehicle. Behind the lawn there are mountains and buildings as well. The first

two Stokes parameters of collection are shown in Fig. 2 (a) and Fig. 2 (b) respectively. Disturbances resulted from the radio frequency interference of the second imaging sensor working simultaneously can be clearly seen around the cab, and the temperature range is adapted to display more details.

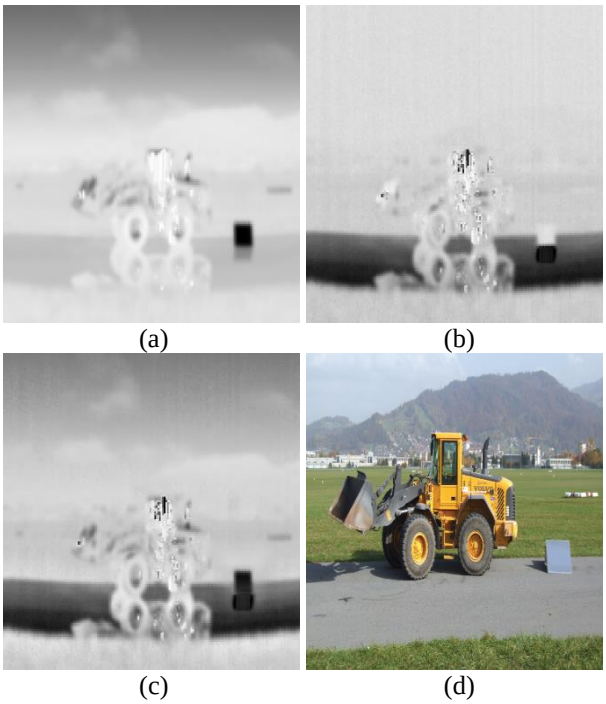

(a) (b) (c) (d)

Fig. 2. Polarimetric MMW imagery and fusion result of a digger. (a) Unpolarized image S_0, (b) polarization difference image S_1, (c) fused polarimetric image, and (d) photo of the imaging scene.

It can be seen in Fig. 2 (a) that the sky and the tilted metal plate have a lower radiometric temperature. The cold temperature of metal plate is resulted by the reflection of sky due to its high reflectivity close to 1. The radiometric temperature of the asphalt road is lower than that of the lawn due to a higher reflectivity. The above results can be explained with the expression of detected radiometric temperature given by:

$$T_a(x,y) = R(x,y)T_{inc}(x,y) + \left[1\text{-}R(x,y)\right]T_{obj}(x,y), \quad (15)$$

where T_a is the radiometric temperature, R denotes the reflectivity, T_{inc} stands for the radiometric temperature incident on the object at the reflection angle, T_{obj} is the kinetic temperature of the object. For the observed scene, radiometric temperature incident on the objects is the radiometric temperature of clear sky which is a cold source. As the reflectivity of the metal plate is close to 1, it is known from the above equation that T_a is almost the same with the radiometric temperature of sky and thus it resulted in a low temperature of the metal plate. Also, it can be concluded from Equation (15) that a higher reflectivity will bring a lower radiometric temperature if two targets have the same kinetic temperatures.

In Fig. 2 (b), radiometric temperature difference between horizontal and vertical states for the asphalt road is higher which is caused by a big Fresnel coefficient difference between the orthogonal states. Also the inverted reflections of the vehicle and the tilted metal plate on the road are also obvious from the both figures. With the proposed fusion method, more details can be found in the fused image compared with the source images.

As shown in Fig. 3 (d), a basin full of water is placed on the lawn and imaged with the polarimetric MMW imaging system. The delivered polarimetric images are presented in Fig. 3 (a) and Fig. 3 (b) respectively.

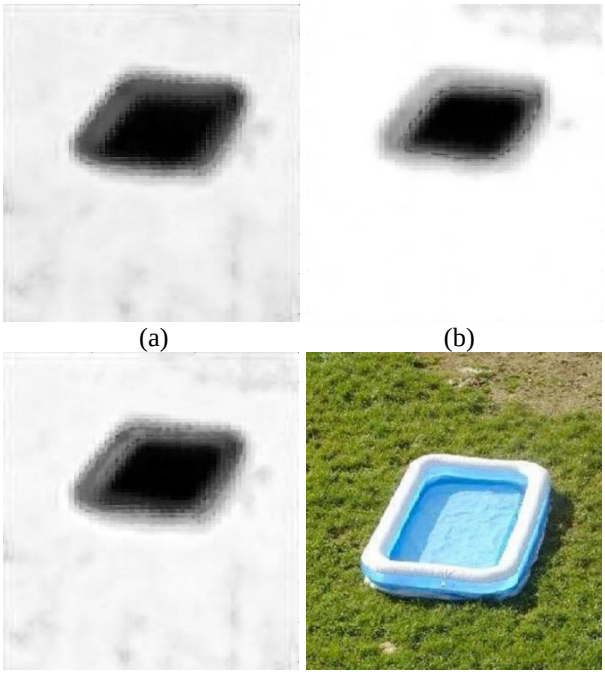

(a) (b) (c) (d)

Fig. 3. Polarimetric MMW imagery and fusion result of a basin. (a) Unpolarized image S_0, (b) polarization difference image S_1, (c) fused polarimetric image, and (d) photo of the imaging scene.

It is seen from the imaging results that the radiometric temperature of water is lower than that of the lawn because it reflects more radiation of the cold sky. Also a big polarization difference is observed for water because the reflectivity difference between horizontal and vertical polarization is larger. And the horizontal radiometric temperature of water is lower due to a lager reflectivity in this polarization. The fused image obtained with the proposed method is shown in Fig. 3 (c). It can

be also found that the fused image provides more details than any single source image.

Though the subject evaluation is a direct and effective method, it varies a lot as this depends on the individuals' experiences. As a result, some metrics such as standard deviation (SD), entropy (EN), mean gradient (MG), and spatial frequency (SF) are employed to evaluate the quality of the fused images objectively.

The standard deviation delivers an overview of the contrast of image. A larger standard deviation means a higher image contrast. In the field of imaging processing, information entropy denotes the average information included in the image. A larger information entropy means a better fusion effect as it provide more details and information in the image. The mean gradient indicates the clarity of image and detailed texture features. The spatial frequency computed in the spatial domain is used to measure the overall activity level of an image.

The objective performances of the proposed fusion method are summarized in Table 1. Also the fusion quality indexes of the multi-scale transform based dual-tree complex wavelet transform (DTCWT) with a decomposition level of 4 [16, 17] and two-scale image fusion using saliency detection (TS-SD) [18] are given for comparison.

Table 1: Quality metrics of various fusion methods for polarimetric MMW imagery

Source Images	Metrics	DTCWT	TS-SD	Proposed
Digger	SD	32.7446	34.4488	47.5733
	MG	3.7212	3.0040	3.7862
	EN	6.6312	6.5985	7.0216
	SF	13.4614	10.4936	13.4021
Basin	SD	63.4588	64.5289	65.5313
	MG	1.8458	1.6210	1.8706
	EN	5.2473	5.3465	5.4157
	SF	7.0857	5.7857	6.8539

As shown in Table 1, the proposed fusion method is able to outperform TS-SD in terms of all quality metrics for the both experiments. The proposed method also has a better performance than DTCWT in most quality indexes except SF. We think that the excellent ability of details preservation contributes a better performance in SF for the DTCWT. Given that the passive MMW imaging sensors suffer from a problem of low resolution compared with high resolution optical imagery, the spatial attention model introduced for fusion weight maps construction plays a significant role to achieve the best performances in most cases for the proposed method.

To evaluate the computational performance of the presented fusion method, the computational time for processing the digger and basin images is summarized in Table 2, and time for DTCWT and TS-SD algorithms is presented for comparison. Experiments are conducted on a computer with 2.6 GHz CPU and 8 GB RAM. The decomposition level of DTCWT is 4 in the experiment. From the above experimental results, it is concluded that two-scale decomposition based methods are more efficient than DTCWT, and the proposed method runs a bit faster than TS-SD.

Table 2: Computational time of various methods

Source Images	Computational Time in Seconds		
	DTCWT	TS-SD	Proposed
Digger	0.219	0.020	0.016
Basin	0.275	0.029	0.022

B. Polarization information display results

Also, the above collected polarimetric passive MMW imagery is dealt with the proposed polarization information display technique. Here the minimum saturation value λ_{sat} is set to 0.3 for a better visual effect. The color images obtained with the proposed method and PDC are presented in Fig.4 and Fig.5 for the digger imagery respectively. The parameters for PDC are chosen with the second method which would produce the most informative images qualitatively [12].

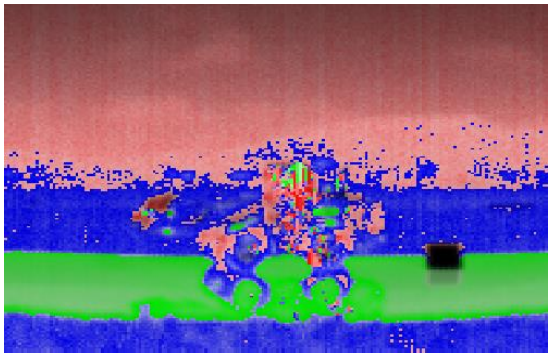

Fig. 4. Polarimetric passive MMW imagery of the digger displayed with the proposed technique.

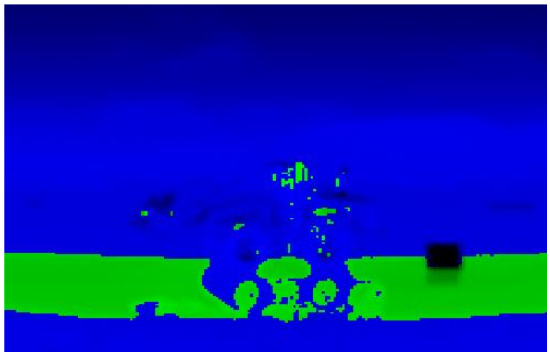

Fig. 5. Polarimetric passive MMW imagery of the digger displayed through PDC.

It can be found from the figures that a color image provides a more intuitive effect as objects are differentiated by color. Compared with PDC, the proposed technique in this paper offers a superior ability of object classification. Moreover, more details are featured with a various color saturation for each classification. Though the lawn is marked with green color, there is a minor difference between the lawn covered and uncovered by the reflection of digger. In addition, the radio frequency interference spots on the digger can be easily distinguished due to the highest saturation level.

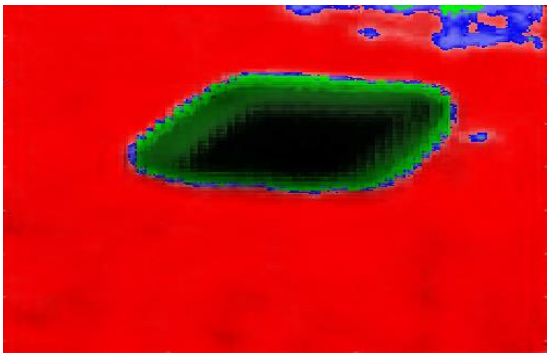

Fig. 6. Polarimetric passive MMW imagery of the basin displayed with the proposed technique.

The color basin polarimetric passive MMW imagery displayed with the proposed method and PDC are presented in Fig. 6 and Fig. 7 respectively. It can be seen from the results that the lawn and gravel ground are separated with different colors by the proposed technique, whereas the difference cannot be distinguished in the color image generated with PDC.

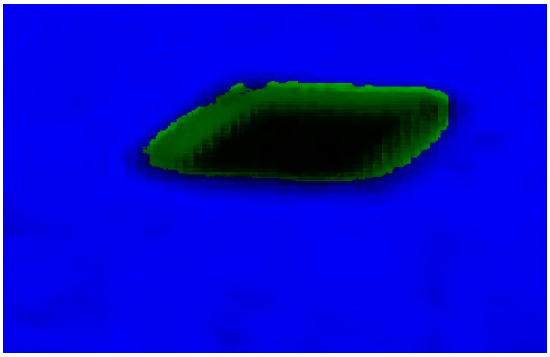

Fig. 7. Polarimetric passive MMW imagery of the basin displayed through PDC.

V. CONCLUSION

As the polarimetric radiation of object provides supplementary information for passive MMW imaging, the post-processing techniques are increasingly significant for polarimetric passive MMW imagery analysis and understanding. The polarimetric imagery fusion method and polarization display technique are discussed in this paper. The performances of the proposed fusion method are better than the methods of DTCWT and TS-SD in terms of objective imagery quality metrics. Additionally, it's simple and computing efficient due to that the two-scale decomposition does not rely on complex image decomposition steps. Also a technique for displaying polarization information through color is presented to provide a more informative image. The unpolarized image can be displayed simultaneously with the polarization. Compared with the conventional PDC technique, the proposed method has a better performance in the object classification and details presentation.

As for the future work, more experiments will be conducted to further verify the performances of the proposed post-processing techniques for polarimetric passive MMW imagery. Additionally, there is a large quality of fusion algorithms which are applied in optical and infrared image processing. More efficient and better fusion methods can be explored to demonstrate the potential of radiometric polarization information application.

ACKNOWLEDGMENT

The authors would like to express their deepest gratitude to Dr. Murk Axel from University of Bern for providing the imaging data. This work was supported by the National Natural Science Foundation of China (No. 61501234), and the Fundamental Research Funds for the Central Universities (No. 30920140122005).

REFERENCES

[1] E. Gonzalez-Sosa, R. Vera-Rodriguez, J. Fierrez, and V. Patel, "Exploring body shape from mmW images for person recognition," *IEEE Trans. Inf. Forensics Security*, vol. 12, pp. 2078-2089, 2017.

[2] L. Wu, S. Peng, Z. Xiao, and J. Xu, "Sensitivity analysis and tipping calibration of a W-band radiometer for radiometric measurements,"*Appl. Comput. Electromagn. Soc. J.*, vol. 31, 2016.

[3] S. Liao, N. Gopalsami, T. W. Elmer, E. R. Koehl, A. Heifetz, K. Avers, E. Dieckman, and A. C. Raptis, "Passive millimeter-wave dual-polarization imagers," *IEEE Trans. Instrum. Meas*., vol. 61, pp. 2042-2050, 2012.

[4] J. P. Wilson, C. A. Schuetz, C. E. Harrity, S. Kozacik, D. L. Eng, and D. W. Prather, "Measured comparison of contrast and crossover periods for passive millimeter-wave polarimetric imagery," *Opt. Express*, vol. 21, pp. 12899-12907, 2013.

[5] A. Duric, A. Magun, A. Murk, C. Matzler, and N. Kampfer, "The fully polarimetric imaging radiometer SPIRA at 91 GHz," *IEEE Trans. Geosci. Remote Sens.*, vol. 46, pp. 2323-2336, 2008.

[6] P. S. Narvekar, G. Heygster, T. J. Jackson, R.

Bindlish, G. Macelloni, and J. Notholt, "Passive polarimetric microwave signatures observed over Antarctica," *IEEE Trans. Geosci. Remote Sens.*, vol. 48, pp. 1059-1075, 2010.

[7] Y. Cheng, F. Hu, L. Gui, L. Wu, and L. Lang, "Polarization-based method for object surface orientation information in passive millimeter-wave imaging," *IEEE Photon. J.*, vol. 8, pp. 1-12, 2016.

[8] F. Hu, Y. Cheng, L. Gui, L. Wu, X. Zhang, X. Peng, and J. Su, "Polarization-based material classification technique using passive millimeter-wave polarimetric imagery," *Appl. Opt.*, vol. 55, pp. 8690-8697, 2016.

[9] S. Yeom, D. Lee, H. Lee, J. Son, and V. P. Gushin, "Vector clustering of passive millimeter wave images with linear polarization for concealed object detection," *Prog. Electromagn. Res. Lett.*, vol. 39, pp. 169-180, 2013.

[10] X. Lu, Z. Xiao, and J. Xu, "Linear polarization characteristics for terrain identification at millimeter wave band," *Chin. Opt. Lett.*, vol. 12, pp. 101201, 2014.

[11] S. Siegenthaler, M. Canavero, and A. Murk, "Post-processing techniques for radiometric images," *IEEE Geoscience and Remote Sensing Symposium*, Munich, pp. 2316-2319, July 2012.

[12] J. P. Wilson, C. A. Schuetz, T. E. Dillon, D. L. Eng, S. Kozacik, and D. W. Prather, "Display of polarization information for passive millimeter-wave imagery," *Opt. Eng.*, vol. 51, pp. 091607, 2012.

[13] S. Li, X. Kang, and J. Hu, "Image fusion with guided filtering," *IEEE Trans. Image Process.*, vol. 22, pp. 2864-2875, 2013.

[14] Y. Zhai and M. Shah, "Visual attention detection in video sequences using spatiotemporal cues," *Proceedings of the 14th ACM International Conference on Multimedia*, Santa Barbara, CA, pp. 815-824, Oct. 2006.

[15] O. Stähli, "Novel Measurements with the Imaging Polarimeter SPIRA (91 GHz) after Technical Upgrades," Master Thesis, Inst. Appl. Physics, University of Bern, Switzerland, 2009.

[16] Y. Liu, S. Liu, and Z. Wang, "A general framework for image fusion based on multi-scale transform and sparse representation," *Inf. Fusion*, vol. 24, pp. 147-164, 2015.

[17] J. J. Lewis, R. J. O'Callaghan, S. G. Nikolov, D. R. Bull, and N. Canagrajah, "Pixel-and region-based image fusion with complex wavelets," *Inf. Fusion*, vol. 8, pp. 119-130, 2007.

[18] D. P. Bavirisetti and R. Dhuli, "Two-scale image fusion of visible and infrared images using saliency detection," *Infrared Phys. Tech.*, vol. 76, pp. 52-64, 2016.

L. Wu received the B.S., M.S. and Ph.D. degrees all in Electrical Engineering from Nanjing University of Science and Technology (NUST), Nanjing, China, in 2003, 2005 and 2009, respectively. Since 2009, he has been a Lecturer with School of Electronic and Optical Engineering at NUST. His research interests involve passive imaging, remote sensing, millimeter wave radar system and application.

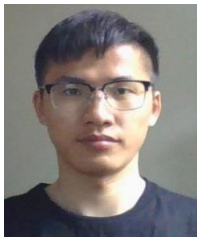

J. Q. Zhu received the B.S. and M.S. degrees all in Electrical Engineering from Nanjing University of Science and Technology (NUST), Nanjing, China, in 2015 and 2018. His research interest is millimeter wave passive imaging.